Ergodic theory and experimental visualization of invariant sets in chaotically advected flows

Igor Mezić[a)]
Division of Engineering and Applied Science, Harvard University, Cambridge, Massachusetts 02138

Fotis Sotiropoulos
School of Civil and Environmental Engineering, Georgia Institute of Technology, Atlanta, Georgia 30332-0355

(Received 11 August 2000; accepted 1 April 2002; published 29 May 2002)

We analyze a recently proposed experimental technique for constructing Poincaré maps in flows exhibiting chaotic advection and develop the theoretical framework that explains the reasons for the success of this approach. The technique is nonintrusive and, thus, simple to implement. Planar laser-induced fluorescence is employed to collect a sufficiently long sequence of instantaneous light intensity fields on the plane of section of the Poincaré map (defined by the laser sheet). The invariant sets of the flow are visualized by time-averaging the instantaneous images and plotting iso-contours of the so resulting mean light intensity field. By linking the Eulerian time averages of light intensity at fixed points in space with the Lagrangian time averages along particle paths passing through these points, we show that ergodic theory concepts can be used to show that this procedure will indeed visualize invariant sets of the Poincaré map. As the technique is based on time-averaging, we discuss the rates of convergence and show that inside regular islands the convergence is fast. An example is presented from the application of this technique to visualize the intricate web of regular islands within a steady, three-dimensional vortex breakdown bubble. © *2002 American Institute of Physics.* [DOI: 10.1063/1.1480266]

I. INTRODUCTION

The complex Lagrangian properties of flows that are simple from the Eulerian point of view—a phenomenon dubbed *chaotic advection* by Aref[1]—have been the subject of intense research in the last 20 years. Even though the very first example of chaotic advection was in a three-dimensional flow,[2,3] most studies in the 1980s focused on two-dimensional, time-periodic flows. Only in the last fifteen years systematic investigations of three-dimensional flows have began to appear in the literature.[4–12] Furthermore, most previous work, both in two- and three-dimensional flows, has been theoretical, and, thus, considerably less progress has been made in the experimental front—see Fountain *et al.*[13] for a review and an interesting recent article by Rothstein *et al.*[14]

The scarcity of experimental work may be partly attributed to the level of abstraction used in theoretical studies to predict the phenomena that occur in chaotically advected flows. Consider for example the concept of the Poincaré map—a powerful dynamical systems tool that can provide important qualitative information about the Lagrangian dynamics of the flow. Poincaré maps can be used to identify well-mixed regions in the flow, reveal the existence of unmixed regular islands, and even provide some information concerning the topology of such islands by revealing their period. The first successful attempt to construct experimental Poincaré maps for a chaotically advected three-dimensional flow was reported only recently by Fountain *et al.*[8,13] Fountain *et al.* employed a series of injection needles to deliver small blobs of dye at various locations within the chaotically advected region of the flow they studied, thus specifying a set of initial ''particle'' locations. The intersections of the resulting streaks of dye with a laser sheet constitute, by definition, the orbit of the Poincaré map of the flow.[8,13] Fountain *et al.*[8,13] applied this technique to a creeping flow in an open cylindrical container driven by a rotating tilted disk and were able to construct experimental Poincaré maps that were in excellent agreement with numerical computations. In spite of their success, however, this technique is not easy to implement and, thus, it might not be suitable for complex three-dimensional flows—see the related discussion in Fountain *et al.*[8] Therefore, further progress in laboratory studies of chaotic advection is hindered by the lack of a simple, nonintrusive experimental technique for visualizing invariant sets of Poincaré maps in two- and three-dimensional flows.

Sotiropoulos *et al.*[15] recently proposed a simple experimental technique for visualizing invariant sets in steady, three-dimensional flows. Their method relies on the standard laser-induced fluorescence (LIF) technique and consists of the following steps: (1) introduce, within the chaotically advected region of the flow, a nonuniform concentration of fluorescent dye at the initial time; (2) illuminate the surface of section of the Poincaré map (a surface that is not tangential to the flow and to which fluid particles starting on the surface return to) with a laser sheet; (3) using digital photography, collect a sufficiently long sequence of LIF images; (4)

[a)]Present address: Department of Mechanical and Environmental Engineering, University of California, Santa Barbara, CA 93106.

time average the instantaneous light intensity fields at the surface of section; and (5) plot the level sets of the resulting mean light intensity field. Sotiropoulos *et al.*[15] have applied this method to construct experimental Poincaré maps for flows within steady vortex breakdown bubbles in a three-dimensional, confined, swirling flow (see Sotiropoulos *et al.*[10] for a numerical treatment of chaotic advection in this flow). Extensive comparisons with numerically constructed Poincaré maps have shown that the iso-contours of the time-averaged light intensity field visualize the invariant sets of the flow with remarkable accuracy.[15] It is important to emphasize, however, that unlike the technique proposed by Fountain *et al.*,[8] whose relation to the Poincaré map of the flow is direct and readily apparent, the link between the technique of Sotiropoulos *et al.*[15] and the theoretical concept of the Poincaré map is far from obvious. In fact, at first glance, there appears to be a fundamental conceptual difference between the definition of the Poincaré map, which relies on the Lagrangian description of the flow, and the technique of Sotiropoulos *et al.*[15] in which the invariant sets are visualized by plotting iso-contours of Eulerian time averages of light intensity—i.e., averages constructed at fixed points in space (the pixels of the digital LIF images). Sotiropoulos *et al.*[15] proposed this technique based on physical intuition and the good agreement they obtained between the experimental and numerical Poincaré maps.

In this work, we analyze the experimental method of Sotiropoulos *et al.*[15] using ergodic theory tools introduced in the studies by Mezić,[16] Mezić and Wiggins,[17] Malhotra *et al.*,[18] and Poje *et al.*,[19] and explain its exact relationship with a Poincaré map of the flow. By linking the Eulerian time averages of light intensity at fixed points in space with the Lagrangian time averages along particle paths, we formally show that the level sets of the time-averaged light intensity field are indeed the invariant sets of the Poincaré map of the flow. We also extend the method to two- and three-dimensional time-periodic flows and, thus, develop the theoretical framework for the first, nonintrusive experimental method for constructing Poincaré maps. It is important to note that the idea of using passive scalar fields to measure velocity of an incompressible flow first appeared in the work of Pearlstein and Carpenter.[20] To the best of our knowledge, however, this is the first time that an Eulerian passive scalar measurement is proposed as the means to visualize Poincaré maps.

The paper is organized as follows: in Sec. II we discuss the concept of invariant sets of a flow and relate it to Poincaré maps. We also show that the above-described experimental procedure reveals invariant sets of the Poincaré map of three-dimensional steady or time-periodic flows. We present a study of the convergence of the time averages in the ''regular'' islands and show that it is fast. In Sec. III we present some experimental and computational evidence for usefulness of the method for three-dimensional, steady vortex breakdown flow together with the experimental convergence results. We discuss the properties and limitations of the method and conclude in Sec. IV.

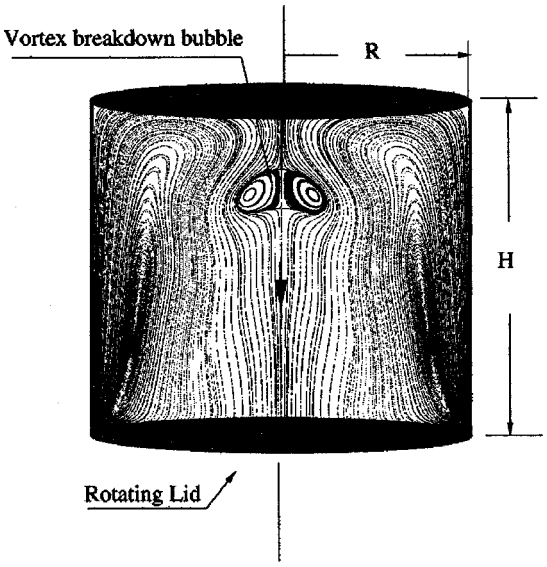

FIG. 1. A schematic of a confined rotating flow.

II. THEORETICAL BACKGROUND FOR THE EXPERIMENTAL METHOD

In this section we develop the theoretical background that establishes the link between the experimental method of Sotiropoulos *et al.*[15] and the Poincaré map of the flow. We begin with a general discussion of the concept of invariant sets and present some ideas from ergodic theory that have been used in the past to numerically visualize invariant sets using Lagrangian time averages. Subsequently we develop the link between Lagrangian time averages and Eulerian time averages and show how the same ergodic theory concepts can be used to develop the theoretical justification for the technique of Sotiropoulos *et al.*[15] Finally, we extend the method to time-periodic two- and three-dimensional flows.

A. The concept of invariant sets

One of the most important concepts in the theory of dynamical systems is that of invariant sets. Assume that the motion of particles in a steady, three-dimensional, incompressible flow contained in a closed domain Ω is given by

$$\begin{aligned} \dot{x} &= v_x(x,y,z), \\ \dot{y} &= v_y(x,y,z), \\ \dot{z} &= v_z(x,y,z). \end{aligned} \tag{1}$$

An invariant set for (1) is a subset $\mathbf{A}$ of Ω that has the following property:

A fluid particle that is at a point (x_0,y_0,z_0) *in* $\mathbf{A}$ *initially (at* $t=0$*) is in* $\mathbf{A}$ *for all positive and negative times.*

In other words, the trajectory of a fluid particle that passes through any (x_0,y_0,z_0) in $\mathbf{A}$ [or equivalently, the streamline—which is equal to the pathline in a steady flow—passing through (x_0,y_0,z_0)] is entirely contained in $\mathbf{A}$.

Some examples of invariant sets include toroidal surfaces on which particles moving in a vortex ring-type flow are confined. If a flow has an integral of motion such as a stream function in three dimensions (for a discussion of its

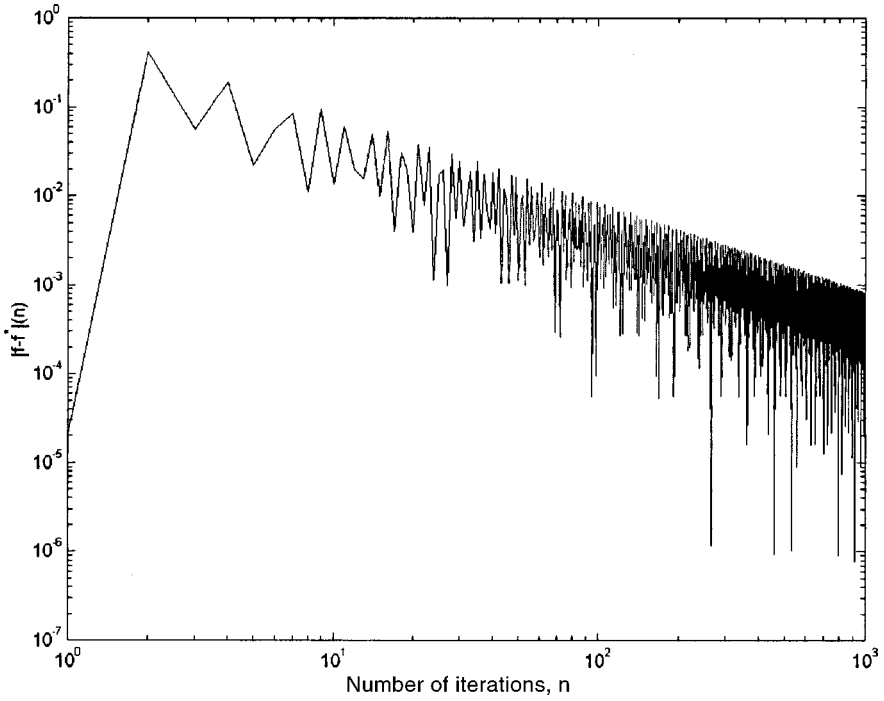

FIG. 2. Convergence of the time average of $f=\sin^2(2\pi x)$ along an orbit of the map $x\to x+\omega$, (mod 1) where $\omega=1/\sqrt{3}$.

existence see Haller and Mezić[21]), every level surface of the stream function is an invariant set. In fact, in that case the three-dimensional flow domain is said to be *foliated* by two-dimensional level-sets of stream surfaces. If the flow exhibits chaotic advection, this type of structure of invariant sets might not exist. Indeed, the fluid particles could possibly explore the whole three-dimensional domain *ergodically*—in which case the only invariant set of positive volume is the whole domain Ω (neglecting sets of zero volume). For most steady and time-periodic three-dimensional flows, the situation is somewhere in between. Namely, two-dimensional toroidal or cylindrical invariant surfaces and chaotic regions that are three-dimensional invariant sets of nonzero volume may be found.

B. Visualization of invariant sets using ergodic theory concepts

Mezić[16] and Mezić and Wiggins[17] have proposed an approach for visualizing invariant sets in numerical studies using the time average f_L^* of a function f (some property of the flow field) over a path line (i.e., the Lagrangian time average of f):

$$f_L^*(\mathbf{X}_0)=\lim_{t\to\infty}\frac{1}{t}\int_0^t f(\mathbf{X}(t,\mathbf{X}_0))\ \ dt, \tag{2}$$

where $\mathbf{X}_0=(x_0,y_0,z_0)$ is the initial condition and $\mathbf{X}=(x(t,\mathbf{X}_0),y(t,\mathbf{X}_0),z(t,\mathbf{X}_0))$ is the solution of (1) passing through $\mathbf{X}_0$ at $t=0$. In the experimental work, we will choose f to be the initial distribution of dye intensity, c_0, and show that the Lagrangian time average of c_0 can be easily measured using LIF.

The average in Eq. (2) exists by the fact that the flow is incompressible and Ω is bounded using Birkhoff's ergodic theorem. Note that Birkhoff's ergodic theorem is valid for almost every initial condition (in the sense of measure theory) and thus its validity is not restricted only to chaotic subdomains or regular subdomains. The level sets of the function f_L^* are in fact invariant sets for the system (1). This is a simply proven fact from ergodic theory (see, e.g., Petersen[22]). Thus, invariant sets can be visualized by:

(1) defining a set of initial conditions $\mathbf{X}_0$,
(2) computing the Lagrangian time averages of a chosen function f over the fluid particle trajectories (streamlines in a steady flow) originating from the points $\mathbf{X}_0$,
(3) mapping the so computed $f_L^*(\mathbf{X}_0)$ to $\mathbf{X}_0$ and plotting the iso-contours of the resulting scalar field on the domain Ω.

We will now show that a simple experimental method can utilize these ergodic theory concepts to visualize the structure of invariant sets in steady and time-periodic flows.

C. Ergodic theory and the experimental method of Sotiropoulos *et al.* (Ref. 15)

The above-mentioned procedure for visualizing invariant sets has been developed for and successfully applied in numerical studies.[16–18] However, the usefulness of this approach in the laboratory is not readily apparent as Lagrangian quantities cannot be easily measured experimentally. Instead in the laboratory we can most commonly only construct Eulerian averages by recording and time averaging a sufficiently long time series of f at a point. In this section we clarify the link between the Lagrangian and Eulerian time averages of f and show how the above-described ergodic theory ideas can be used to formally explain the reasons for the success of the experimental method of Sotiropoulos *et al.*[15]

Consider a steady flow in the rotating cylinder as shown

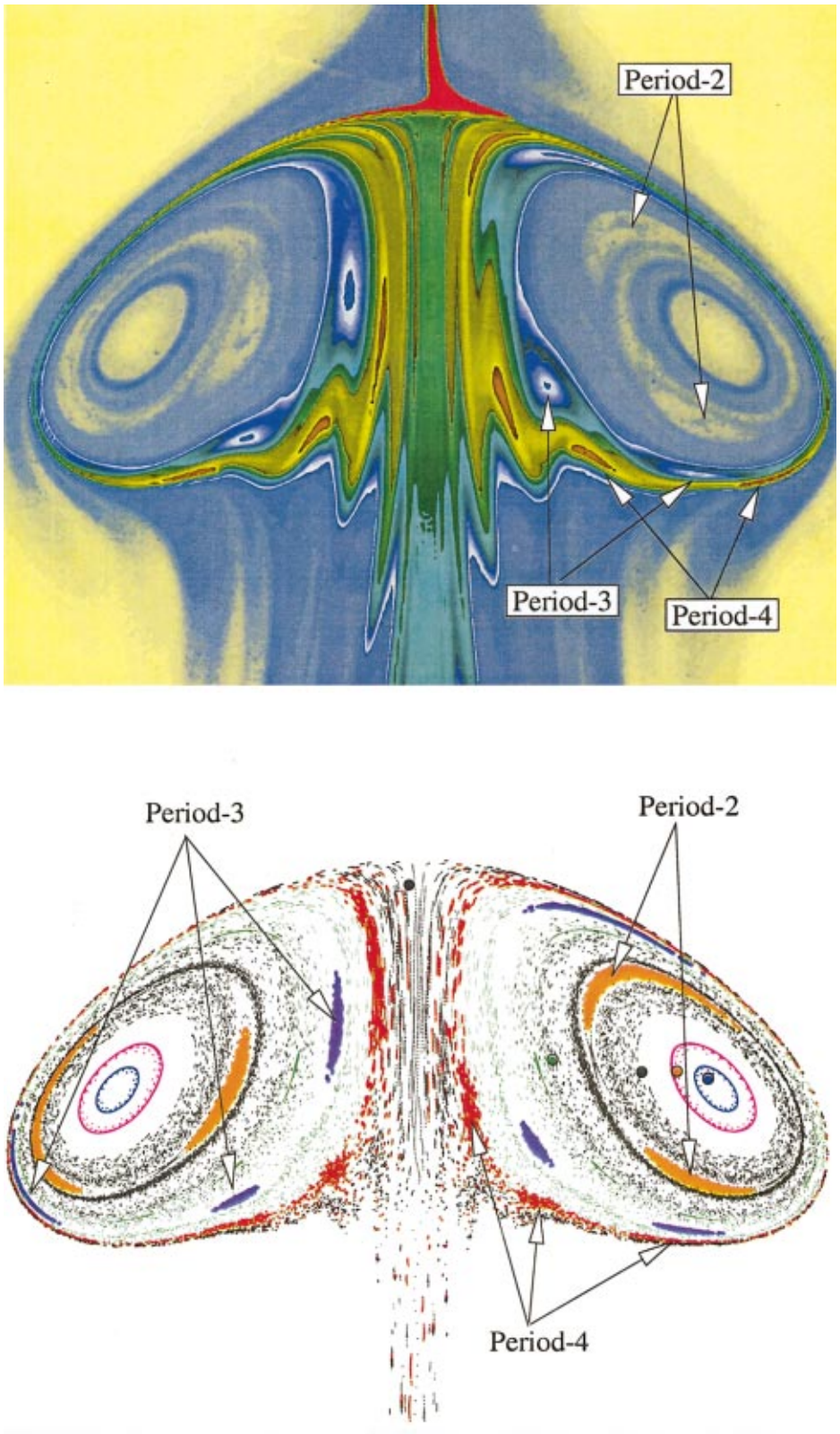

FIG. 3. (Color) Experimental (Ref. 15) and calculated (Ref. 10) Poincaré maps for a steady vortex breakdown bubble ($H/R=1.75$, $\mathrm{Re}=1850$). The experimental map was constructed by plotting the level sets of the time-averaged light-intensity field. For the calculated map, same-color markers were released along short straight segments, selectively placed within various regions in the interior of the bubble to elucidate the richness of the dynamics. Note the level of agreement between the two images in terms of both the period and relative location of the various invariant sets.

in Fig. 1. Fix a diametral plane Σ that contains the cylinder axis. For a rotating flow, a Poincaré map P can be defined as the map that sends $\mathbf{X}_0$ to the first intersection of the trajectory passing through $\mathbf{X}_0$ with Σ. Invariant sets for Poincaré maps are the intersections of invariant sets for the flow (1) with the plane Σ. To clarify the relationship between the so-constructed Poincaré map of the flow and the iso-contours of the time-averaged light intensity field, let fluorescent dye be distributed in Ω at time $t=0$ with a nonuniform concentration $c_0(x,y,z)$—in LIF experiments the concentration of fluorescent dye is linearly proportional to the intensity of emitted light, which can be readily quantified using digital photography. Assume the concentration of dye is advected perfectly by the flow (i.e., there is no diffusion) and de-

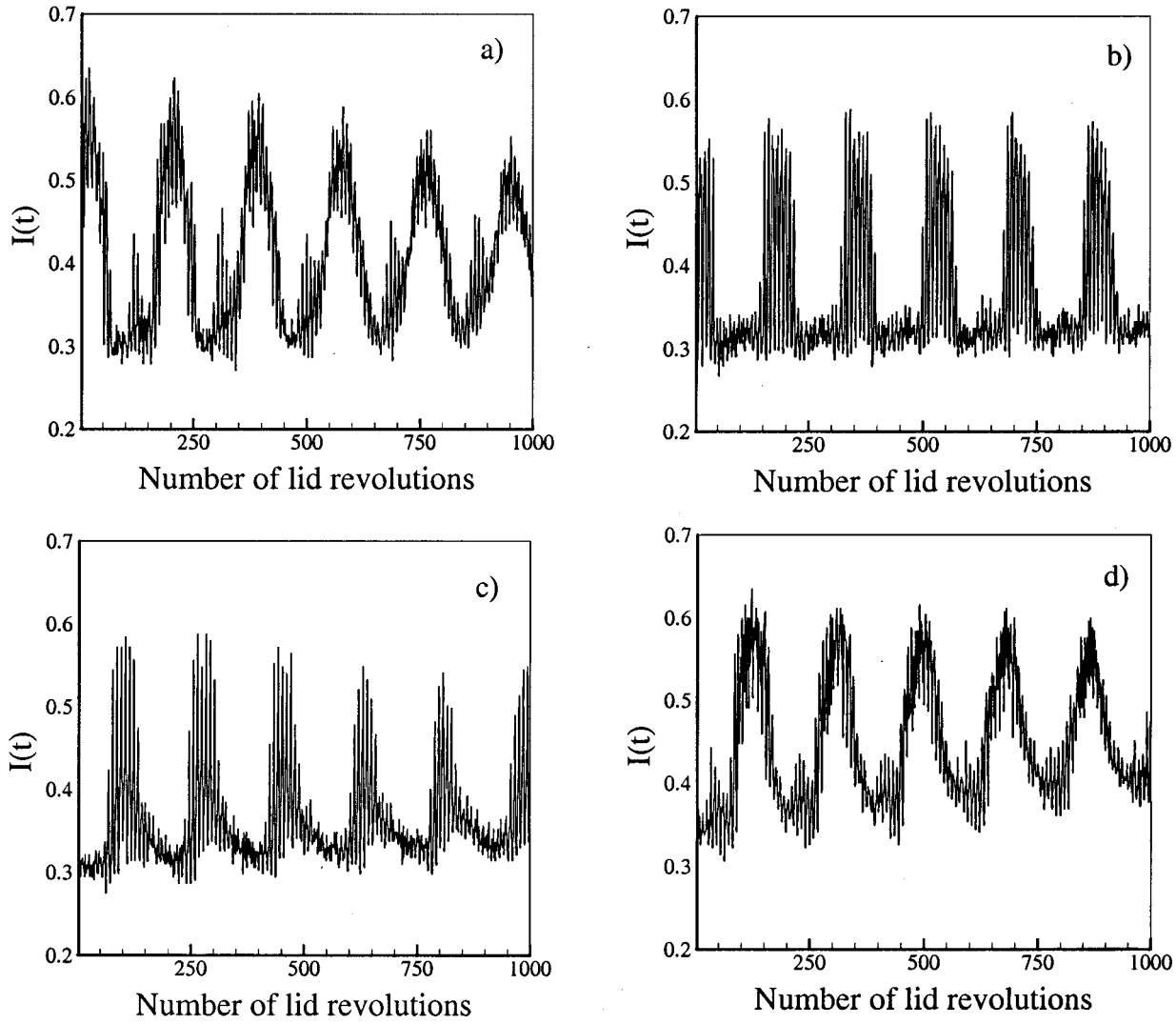

FIG. 4. Experimental signals of light intensity at four points within the vortex breakdown bubble shown in Fig. 3. Points (a), (b), and (c) are within the internal invariant core of the bubble while point (d) is within the period-two island.

scribed by a function $c(x,y,z,t)$ such that $c(x,y,z,0) = c_0(x,y,z)$. The advection of dye is described by

$$\frac{\partial c}{\partial t} + \nu_x \frac{\partial c}{\partial x} + \nu_y \frac{\partial c}{\partial y} + \nu_z \frac{\partial c}{\partial z} = 0. \tag{3}$$

The solution of (3) can be written explicitly as

$$c(x,y,z,t) = c_0(\Phi^{-t}(x,y,z)),$$

where $\Phi^s(X_0)$ is the position at time s of a fluid particle that is at the point $\mathbf{X}_0$ at time $t=0$.

Consider a point p in Σ. The Eulerian time average of c at p is given by

$$c_{\mathrm{E}}^*(p) = \lim_{t\to\infty} \frac{1}{t} \int_0^t c(p,t)\,dt.$$

Note that by time averaging a sequence of instantaneous light intensity fields, Sotiropoulos *et al.*[15] in essence calculated Eulerian averages of light intensity (and, thus, concentration) at all points (pixels of the digital image) on Σ, which in the laboratory is defined by the laser sheet. The following calculation shows that $c_{\mathrm{E}}^*(p)$ is in fact equal to the time average of the concentration along the trajectory passing through p, i.e., the Lagrangian time average of c:

$$c_{\mathrm{E}}^*(p) = \lim_{t\to\infty} \frac{1}{t} \int_0^t c(p,t)\,dt = \lim_{t\to\infty} \frac{1}{t} \int_0^t c_0(\Phi^{-t}p)\,dt = c_{\mathrm{L}}^*(p). \tag{4}$$

The last equality follows from the fact that the time average over negative time is equal to the time average over positive time for incompressible flows—by the invertibility of Φ^s.[23]

Equation (4) places us now firmly in the context of the previously discussed ergodic theory ideas and allows for a clear interpretation of the experimental technique developed by Sotiropoulos *et al.*[15] in terms of the Lagrangian visualization method of Mezić[16] and Mezić and Wiggins.[17] Since the Eulerian time averages of light intensity at fixed points in space are equal to the Lagrangian time averages of light intensity along the particle paths that originate from these points, it follows from our discussion in the previous section

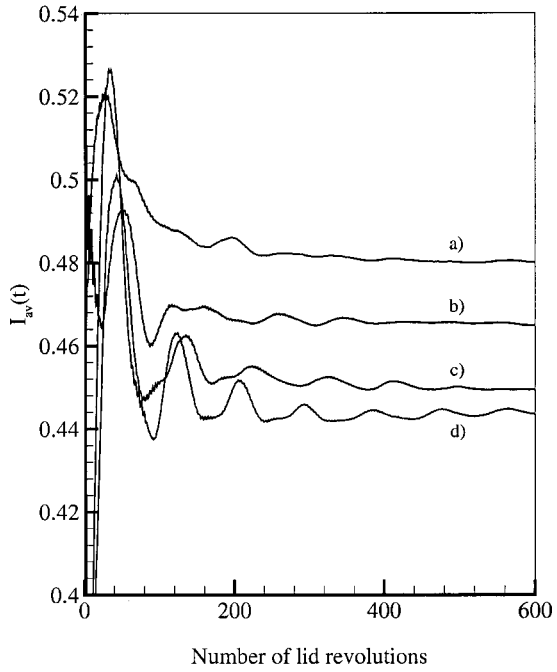

FIG. 5. The convergence of the time-averaged signals from Fig. 4.

that the level sets of the mean light intensity field will indeed visualize the invariant sets of the Poincaré map of the flow. Of course, different initial distributions of dye will give different levels of resolution of invariant sets. At one extreme, a constant c_0 will have the same time average for all initial conditions in the domain and, thus, reveal the fact that the whole domain is an invariant set—not a very useful conclusion. Thus, the concentration at the beginning of the experiment, c_0, has to be nonuniform for good resolution of invariant sets.

D. Convergence times and rate of convergence

An important question that arises in the context of the experimental technique of Sotiropoulos *et al.*[15] is with regard to the length of the averaging time needed for statistically converged results to be obtained, as it is well known that there is no uniformity in the convergence of time averages.[22] This question is related to the issue of "stickiness" of regular islands, where initial conditions close to the islands tend to stay there for a long time, and the accompanying issue of the so-called Levy flights.[24] Meiss,[25] for instance, examined the behavior of one orbit in a positive area ergodic component of the Standard Map and found that only after as many as 10^{10} iterations does the orbit closely exhibit ergodic behavior. If such excessive times were indeed required to obtain converged averages everywhere in the flow, the present experimental technique would obviously be impractical to use. Molecular diffusion would begin to smear the gradients in the light intensity field, thus, making the visualization of the invariant sets impossible. Fortunately, however, convergence inside low-period islands is very rapid.[17] Since, the objective of the present experimental technique is to visualize the invariant sets of the flow, the time interval over which data need to be collected and averaged in the laboratory should be considerably less than the diffusive time scale. Experimental evidence establishing the validity of this conclusion is presented in Sec. III.

An exact theoretical result for the rate of convergence of the time average of a function f can be derived for the special case of periodic orbits of the Poincaré map. Consider an orbit of period q, such that $x^q=x$, where x is a point in the flow domain and x^q denotes the qth iterate of the map starting at x. The time average, $f^*(n)$, of f along the orbit after n iterations of the map $T^i(x)$ is given by

$$f^*(n)=\frac{1}{n}\sum_{i=0}^{n-1} f(T^i(x)) = \frac{1}{n}\left\{\left(\sum_{i=0}^{q-1} f(T^i(x))\right)\left[\frac{n}{q}\right]+\sum_{i=[n/q]q}^{n-1} f(T^i(x))\right\}, \tag{5}$$

where $[n/q]$ is the integer part of n/q. As $n\to\infty$, $f^*(n)\to f^*$ (the converged time average of f) and a bound on the rate of convergence can be calculated as follows:

$$|f^*-f^*(n)|=\left|f^*\left(1-\frac{1}{n}\left[\frac{n}{q}\right]q - \frac{1}{f^*n}\sum_{i=[n/q]q}^{n-1} f(T^i(x))\right)\right|. \tag{6}$$

Note that $[n/q]=n/q-(n/q)'$, where $0\leqslant(n/q)'<1$, and, due to the periodicity of the motion,

$$\left|\sum_{i=[n/q]q}^{n-1} f(T^i(x))\right| = \left|\sum_{i=0}^{n-1-[n/q]q} f(T^i(x))\right| \leqslant \sum_{i=0}^{q-1}|f(T^i(x))|\leqslant\left|\max_q(f)\right|q,$$

where $\max_q(f)$ is the maximum of the function over the orbit. Thus (6) becomes

$$|f^*-f^*(n)|=\left|f^*\left(1-\frac{1}{n}\left(\frac{n}{q}-\left(\frac{n}{q}\right)'\right)q - \frac{1}{n}\sum_{i=[n/q]q}^{n-1} f(T^i(x))\right)\right| \leqslant \frac{|f^*|q}{n}\left(\frac{n}{q}\right)'+\frac{\left|\max_q(f)q\right|}{n} \leqslant \frac{\left(|f^*|+\left|\max_q(f)\right|\right)q}{n},$$

which goes to zero when $n\to\infty$.

For almost periodic orbits, such as those on invariant tori the situation is similar: the rate of convergence of the time averages will in general be bounded above by c/n for some constant c as can be shown by a spectral argument.[26] As an example of this result, we show in Fig. 2 a log–log plot of $|f^*-f^*(n)|$ for a function $f=\sin^2(2\pi x)$ averaged along an orbit of the map T that is a translation on the circle of length

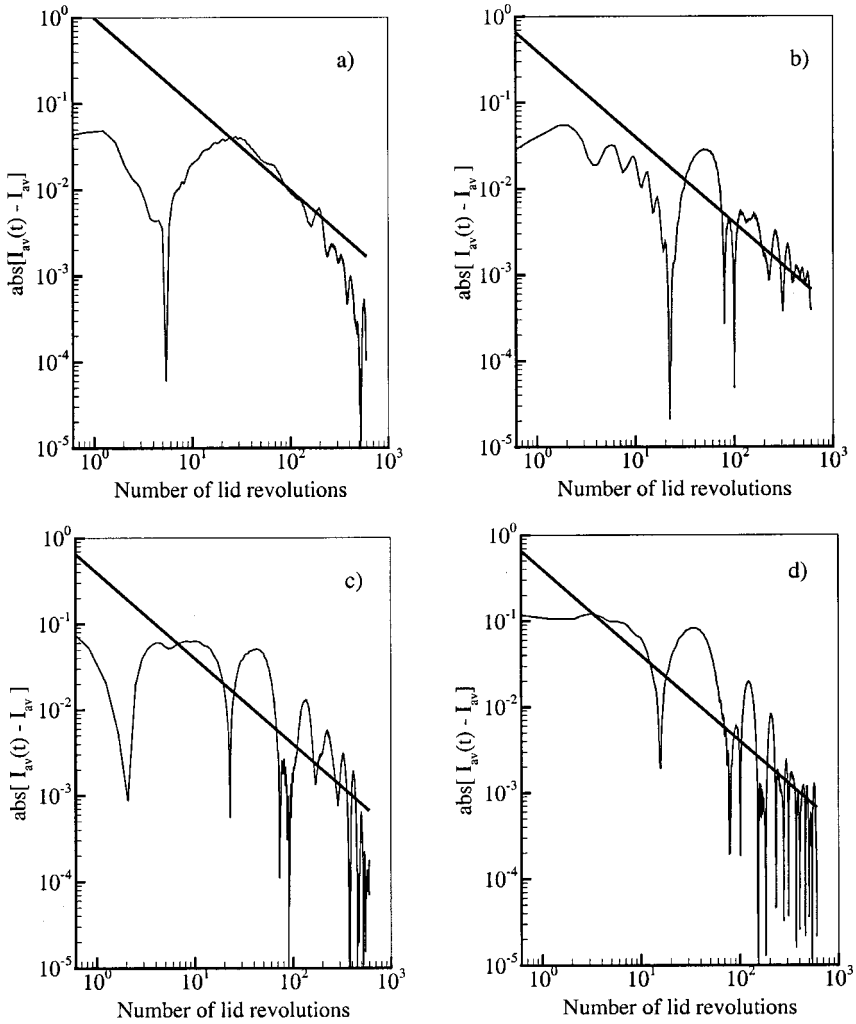

FIG. 6. Log–log plot of the absolute value of the deviation of the time-averaged signal from the mean for the signals shown in Fig. 4. The slope of the straight black line in all plots is equal to -1.

1, $T:x\to x+\omega,(\mathrm{mod}\,1)$, where $\omega=1/\sqrt{3}$. The power-law bound on the convergence rate is clear and the slope is very close to 1.

A similar calculation can be done for the Lagrangian time averages in the continuous-time case. As we have already established the equivalence of Lagrangian and Eulerian time averages, we would anticipate that the experimentally constructed Eulerian time averages of light intensity should in general converge as t^{-1} (in fact, strictly speaking the convergence will be bounded above by c/t) at pixels located within regular invariant sets of the Poincaré map. Experimental results presented in Sec. III support the validity of this conclusion.

For pixels located within chaotic zones we expect much slower convergence: $n^{-1/2}$ due to central-limit type theorems for dynamical systems, or worse. However, fast layering of dye by advection in these regions means that dye mixing will be enhanced and help convergence.

E. Constructing experimental Poincaré maps in time-periodic flows

In this section, we extend the above-mentioned ideas to a time-periodic flow with period τ. The Poincaré map in this case is given by a volume-preserving map T that takes an initial condition (x_0,y_0,z_0) and associates with it the position of the fluid particle starting from that initial condition after one period of time.

Let us assume again that the initial distribution of dye is given by $c_0(x,y,z)$. In this case the averaging of the concentration at any point p of Ω has to be done at multiples of the period:

$$c_{\mathrm{E}}^{*}(p)=\lim_{n\to\infty}\frac{1}{n}\sum_{i=0}^{n-1}c(p,i\tau)=\lim_{n\to\infty}\frac{1}{n}\sum_{i=0}^{n-1}c_0(T^{-i}p)=c_0^{*}, \tag{7}$$

where c_0^* is the average of the initial concentration over the trajectory of the Poincaré map T. The last statement is again based on the fact that for discrete dynamical systems that preserve volume, forward time averages over trajectories are equal to backward (in time) time averages over trajectories. Changing the initial time of the averaging within one period corresponds to changing the phase of the invariant sets for the Poincaré map.

The above-stated convergence results are again valid and inside regular islands, the convergence rate for the Lagrangian very close to $1/n$.

III. AN EXAMPLE: STEADY VORTEX BREAKDOWN BUBBLE IN A CONFINED FLOW

The above-described experimental method has been successfully applied by Sotiropoulos *et al.*[15] to construct, for the first time, Poincaré maps for the flow within steady vortex breakdown bubbles in a confined swirling flow. Since this work has yet to be published, we present herein a small sample of the experimental results obtained by Sotiropoulos *et al.*[15] in order to illustrate the ability of the method to resolve the invariant sets of Poincaré maps. An extensive description of the experiment along with detailed parametric studies and discussion of the dynamics of vortex breakdown flows will be presented in Sotiropoulos *et al.*[15] In addition, we present the convergence results that do not appear elsewhere.

Consider a closed cylinder filled with an incompressible Newtonian fluid of kinematic viscosity ν (see Fig. 1). The bottom end wall is rotated at a constant angular velocity Ω while the top wall is held stationary. The two nondimensional parameters that determine the various flow regimes are the aspect ratio, H/R, and the Reynolds number $\mathrm{Re}=\Omega R^2/\nu$. Ekman suction and pumping drive a meridional flow and give rise to the formation of a columnar vortex along the container axis. Above a threshold Re, this vortex breaks down and forms one or more vortex breakdown bubbles.[27] In a recent experiment, Spohn *et al.*[28] showed that the flow in the steady regime is three-dimensional due to nonaxisymmetric modes that originate inside the sidewall boundary layer. These disturbances perturb the columnar vortex along the axis and lead to vortex breakdown bubbles that are steady, open, and asymmetric at their downstream end.[28] Sotiropoulos and Ventikos[29] studied the same problem numerically by solving the three-dimensional Navier–Stokes equations. They reproduced the laboratory observations of Spohn *et al.*[28] and showed that the flow within stationary vortex breakdown bubbles exhibits chaotic particle paths. A detailed description of the topological aspects of vortex breakdown including a discussion of the specific chaos-inducing mechanism can be found in Sotiropoulos and Ventikos[29] and Sotiropoulos *et al.*[10]

To elucidate the dynamics in the interior of steady, vortex breakdown bubbles, Sotiropoulos *et al.*[10,15] constructed numerical and experimental Poincaré maps. A representative sample of their results (for $H/R=1.75$ and $\mathrm{Re}=1850$) is shown in Fig. 3. The numerical maps were constructed by calculating the trajectories of several initial conditions over long time intervals using a fourth-order accurate Runge–Kutta method and a trilinear spatial interpolation scheme. The steady velocity field was obtained by marching in time the three-dimensional, unsteady Navier–Stokes equations with a finite-volume numerical method that is second-order accurate in both space and time. The results shown in Fig. 3(b) were obtained on a very fine computational mesh, consisting of approximately 1.4×10^6 grid nodes. The details of the numerical method can be found in Sotiropoulos and Ventikos[30] and extensive validation of computations for the container flow are included in Sotiropoulos and Ventikos.[29]

The experimental map was constructed by Sotiropoulos *et al.*[15] by applying the visualization method described herein. The experiments were conducted using a rigid acrylic cylinder with inner diameter of 203 mm. The bottom end wall rotated at speeds up to 140 rpm, driven by a variable-speed dc motor. The gap between the rotating disk and the cylinder wall was less than 0.3 mm. The disk surface rotated smoothly with variation less than 0.025 mm. The working fluid was a water and glycerin mixture (roughly 56% glycerin by weight). The cylinder was mounted in a square tank (305 mm per side) filled with the working fluid to a level slightly higher than the top of the test cell. The temperature of the reservoir fluid was monitored continuously and did not vary more than a few tenths of a degree over several hours of experiments. Fluorescent dye (Rhodamine 6G), dissolved in a sample of glycerin/water mixture, was injected into the container through a 1 mm hole at the center of the stationary cover. A 1-mm-thick diametral slice through the container centerline was illuminated using a pulsed Nd:YAG laser and the emitted light was captured using a digital camera. Instantaneous LIF images were collected at a rate of 1 frame/s over a period of 24 min (the container lid rotates at 0.87 revolutions/s). Instantaneous light intensity fields were collected at a rate of 1 frame/s over a period of 24 min (for this Reynolds number the container lid rotates at 0.87 revolutions/s) using digital photography. Only the first 100 of those images were time averaged, thus providing a discrete approximation to the time average of the concentration in Eq. (4), since averaging over longer time intervals was found to produce essentially the same result. Molecular diffusion effects did not become significant even when the averaging was carried out over the entire 24 min interval.

As seen in Fig. 3, the numerical simulations and laboratory visualizations are in excellent agreement. Both reveal the presence of period two, three, and four islands (invariant sets) embedded within well-stirred stochastic regions (uniform colored regions in the experimental map). This level of agreement along with the theoretical ideas presented herein, validate the proposed visualization technique, and underscore its potential as a powerful tool for experimental investigations of a variety of flows exhibiting chaotic advection.

To illustrate the rapid convergence of the time averages of light intensity within invariant sets of the flow, we show in Fig. 4 experimental signals of light intensity at four points within the vortex breakdown bubble shown in Fig. 3. One of these points is located within the period-two island shown in Fig. 3 while the other three points are located within the internal invariant core of the bubble, which according to the computations consists of periodic and quasiperiodic KAM-tori. The periodic nature of the signals is clear, with a slight diffusive decay evident at this time scale. The convergence of the time-averaged signals from Fig. 4 is shown in Fig. 5 and as seen all signals converge within less than 600 lid rotations. In Fig. 6, log–log plot of the absolute value of the deviation of the time-averaged signal from the mean is shown. For all cases the asymptotic decay rate is bounded above by the $1/n$ rate predicted by the theory.

IV. SUMMARY AND CONCLUSIONS

We have used ergodic theory tools to develop a rigorous theoretical framework for a recently developed experimental technique for visualizing nonergodic regions of mixing in three-dimensional fluid flows. We have also extended the method to time-periodic two- and three-dimensional flows. In light of the elaborate experimental procedures used in the past, the present technique is strikingly simple. Furthermore, it is nonintrusive and thus applicable to a broad range of chaotically advected flows. We anticipate, therefore, this technique to serve as the catalyst for future advances in the theory of chaotic mixing in three-dimensional flows, an area in which progress has long been hindered by the lack of simple procedures for visualizing chaos in the laboratory.

It is important to recognize that there are two prerequisites for successful visualizations of invariant sets with the present technique: (1) the initial spatial distribution of fluorescent dye within the chaotically advected region must be nonuniform; and (2) the averaging time must be smaller than the molecular diffusion time scale of the flow but bigger than a characteristic time scale in steady flows (determined by the lid rotational speed in the present example) or one time period in flows that are periodic in time. More advanced procedures can be designed to utilize the possibility of different nonhomogeneous initial distributions following the theory of ergodic partitions.[16,17]

ACKNOWLEDGMENTS

The digital images used to construct the Poincaré map shown in Fig. 3(a) were obtained by D. R. Webster. F.S. was partially supported by NSF CAREER Award No. CMS-9875691. I.M. was partially supported by NSF Grant No. DMS-9803555 and the Sloan Fellowship.

[1]H. Aref, ''Stirring by chaotic advection,'' J. Fluid Mech. **143**, 1 (1984).
[2]V. I. Arnold, ''Sur la topologie des ecoulements stationaries des fluides-parfait,'' C.R. Acad. Sci. Paris **261**, 17 (1965).
[3]M. Henon, ''Sur la topologie des lignes de courant dans un cas particulier,'' C.R. Acad. Sci. Paris A **262**, 312 (1966).
[4]T. Dombre, U. Frisch, J. M. Greene, M. Henon, A. Mehr, and A. M. Soward, ''Chaotic streamlines in ABC flows,'' J. Fluid Mech. **167**, 353 (1986).
[5]G. M. Zaslavsky, R. Z. Sagdeev, and A. A. Chernikov, ''Stochastization of current lines in stationary flows,'' Zh. Éksp. Teor. Fiz. **94**, 102 (1988).
[6]M. Feingold, L. P. Kadanoff, and O. Piro, ''Passive scalars, three-dimensional volume-preserving maps, and chaos,'' J. Stat. Phys. **50**, 529 (1988).
[7]P. Ashwin and G. P. King, ''Streamline topology in eccentric Taylor vortex flow,'' J. Fluid Mech. **285**, 215 (1995).
[8]G. O. Fountain, D. V. Khakhar, I. Mezić, and J. M. Ottino, ''Chaotic mixing in a bounded 3D flow,'' J. Fluid Mech. **417**, 265 (2000).
[9]H. E. Lomeli and J. D. Meiss, ''Quadratic volume-preserving maps,'' Nonlinearity **11**, 557 (1998).
[10]F. Sotiropoulos, Y. Ventikos, and T. C. Lackey, ''Chaotic advection in three-dimensional vortex breakdown bubbles: Sil'nikov's chaos and the devil's staircase,'' J. Fluid Mech. **444**, 257 (2001).
[11]H. A. Stone, A. Nadim, and S. H. Strogatz, ''Chaotic streaklines inside drops immersed in steady linear flow,'' J. Fluid Mech. **232**, 629 (1991).
[12]A. N. Yannacopoulos, I. Mezić, G. Rowlands, and G. P. King, ''Eulerian diagnostics for Lagrangian chaos in three-dimensional Navier–Stokes flows,'' Phys. Rev. E **57**, 482 (1998).
[13]G. O. Fountain, D. V. Khakhar, and J. M. Ottino, ''Visualization of three-dimensional chaos,'' Science **281**, 683 (1998).
[14]D. Rothstein, E. Henry, and J. P. Gollub, ''Patterns in transient chaotic fluid mixing,'' Nature (London) **401**, 770 (1999).
[15]F. Sotiropoulos, D. R. Webster, and T. C. Lackey, ''Experimental studies of Lagrangian transport in steady vortex breakdown bubbles in a confined flow,'' to be published in J. Fluid Mech.
[16]I. Mezić, Ph.D. thesis, California Institute of Technology, 1994.
[17]I. Mezić and S. Wiggins, ''A method for visualization of invariant sets of dynamical systems based on the ergodic partition,'' Chaos **9**, 213 (1999).
[18]N. Malhotra, I. Mezić, and S. Wiggins, ''Patchiness: A new diagnostic for Lagrangian trajectory analysis in time-dependent fluid flows,'' Int. J. Bifurcation Chaos Appl. Sci. Eng. **8**, 1053 (1999).
[19]A. C. Poje, G. Haller, and I. Mezić, ''The geometry and statistics of mixing in aperiodic flows,'' Phys. Fluids **11**, 2963 (1999).
[20]A. J. Pearlstein and B. N. Carpenter, ''On the determination of solenoidal or compressible velocity-fields from measurements of passive or reactive scalars,'' Phys. Fluids **7**, 754 (1995).
[21]G. Haller and I. Mezić, ''Reduction of three-dimensional, volume-preserving flows by symmetry,'' Nonlinearity **11**, 319 (1998).
[22]K. Petersen, *Ergodic Theory* (Cambridge University Press, Cambridge, 1983).
[23]R. Mane, *Ergodic Theory and Differentiable Dynamics* (Springer, New York, 1987).
[24]M. F. Shlesinger, G. M. Zaslavsky, and J. Klafter, ''Strange kinetics,'' Nature (London) **363**, 31 (1993).
[25]J. D. Meiss, ''Transient measures in the standard map,'' Physica D **74**, 254 (1994).
[26]A. G. Kachurovskii, ''The rate of convergence in ergodic theorems,'' Russ. Math. Surveys **51**, 653 (1996).
[27]M. P. Escudier, ''Observations of the flow produced in a cylindrical container by a rotating end wall,'' Exp. Fluids **24**, 189 (1984).
[28]A. Spohn, M. Mory, and E. J. Hopfinger, ''Experiments on vortex breakdown in a confined flow generated by a rotating disk,'' J. Fluid Mech. **370**, 73 (1998).
[29]F. Sotiropoulos and Y. Ventikos, ''The three-dimensional structure of confined swirling flows with vortex breakdown,'' J. Fluid Mech. **426**, 155 (2001).
[30]F. Sotiropoulos and Y. Ventikos, ''Transition from bubble-type vortex breakdown to columnar vortex in a confined swirling flow,'' Int. J. Heat Fluid Flow **19**, 446 (1998).